High-field phase transitions in the orbitally ordered multiferroic GeV4S8

V. Felea, P. T. Cong, Lilian Prodan, D. I. Gorbunov, T. Nomura, Y. Skourski, S. Zherlitsyn, J. Wosnitza, Zhaosheng Wang, A. Miyata, O. Portugall, Sebastian Widmann, Hans-Albrecht Krug von Nidda, Joachim Deisenhofer, Vladimir Tsurkan, Alois Loidl

High-field phase transitions in the orbitally ordered multiferroic GeV$_4$S$_8$

V. Felea,[1,2] P. T. Cong,[2] L. Prodan ●,[1] D. I. Gorbunov,[2] T. Nomura,[2] Y. Skourski,[2] S. Zherlitsyn ●,[2]
J. Wosnitza,[2] Zhaosheng Wang,[2,3] A. Miyata,[2,4] O. Portugall,[4] S. Widmann,[5] H.-A. Krug von Nidda,[5]
J. Deisenhofer,[5] V. Tsurkan ●,[1,5,*] and A. Loidl ●[5]

[1]*Institute of Applied Physics, MD 2028, Chisinau, Republic of Moldova*
[2]*Hochfeld-Magnetlabor Dresden (HLD-EMFL), Helmholtz-Zentrum Dresden-Rossendorf,
and Würzburg-Dresden Cluster of Excellence ct.qmat, D-01328 Dresden, Germany*
[3]*High Magnetic Field Laboratory, Chinese Academy of Sciences, 230031 Hefei, China*
[4]*Laboratoire National des Champs Magnétiques Intenses, (LNCMI-EMFL), CNRS-UGA-UPS-INSA, 31400 Toulouse, France*
[5]*Experimental Physics V, Center for Electronic Correlations and Magnetism, Institute of Physics,
University of Augsburg, D-86159 Augsburg, Germany*

The high-field (H,T) phase diagram of the multiferroic lacunar spinel GeV$_4$S$_8$ has been studied by ultrasound, magnetization, and pyrocurrent experiments in magnetic fields up to 60 T. The title compound consists of molecular building blocks, with vanadium V$_4$ clusters characterized by a unique electron density. These vanadium tetrahedra constitute a Jahn-Teller active entity, which drive an orbital-ordering transition at 30 K with the concomitant appearance of ferroelectricity. Ultrasound and magnetization experiments reveal sharp anomalies in magnetic fields of 46 T, which are associated with a first-order phase transition into an orbitally disordered state characterized by significant field and temperature hystereses. We report a sequence of complex magnetic, polar, and orbitally ordered states, i.e., the appearance of two orbitally ordered phases OO1 and OO2 for $\mu_0 H < 45$ T and $T < 30$ K. Beyond the paraelectric phase we further evidenced three ferroelectric phases, FE1, FE2, and FE3. Finally, antiferromagnetic (AFM) order ($T < 15$ K) and fully polarized ferromagnetic order ($\mu_0 H > 60$ T) have been observed in GeV$_4$S$_8$. At low temperatures and for fields below 40 T, AFM order coexists with the polar phase FE3 identifying a multiferroic state. Our results demonstrate a fascinating competition of the different orders, which the material manifests in high magnetic fields and at low temperatures.

I. INTRODUCTION

Lacunar spinels represent a large material class of ternary chalcogenides with composition AM_4X_8 ($A =$ Ga and Ge; $M =$ V, Mo, Nb and Ta; $X =$ S and Se). These compounds originate from the normal spinel structure AM_2X_4 with $Fd\bar{3}m$ symmetry by removing one-half of the tetrahedral A-site cations. This A-site deficiency combined with slight structural rearrangements results in the formation of a noncentrosymmetric fcc lattice of $F\bar{4}3m$ symmetry with weakly linked cubane $(M_4X_4)^{n+}$ and tetrahedral $(AX_4)^{n-}$ clusters [1–3]. These molecular units reveal a unique electron density and can be described by a well-defined molecular orbital scheme [4]. Dominated by correlation effects and Mott physics, this class of materials manifests a plethora of topical and exotic effects, including superconductivity [5], metal-to-insulator transitions [6,7], negative magnetoresistance [8], electric field-induced resistive switching [9–11], orbital order-induced ferroelectricity [12–14], multiferroicity [12–18], and skyrmion-lattice formation [19,20]. In addition, the Néel-type skyrmions in bulk lacunar spinels are dressed with ferroelectric (FE) polarization [13,16]. This rich physics of lacunar spinels is of gen-

eral fundamental interest as well as of potential importance for applications in future telecommunication and computer technologies.

Cubanelike metallic clusters with partly filled electronic shells are Jahn-Teller active: For example, in GeV$_4$S$_8$, a singlet, a doublet, and a triplet, with an overall splitting of ~2.9 eV, are occupied by eight electrons and characterize the electronic structure of the V$_4$ cluster of the cubane unit [3]. Two unpaired electrons in the highest triplet constitute a total spin of $S = 1$ [3,21] and this electronic configuration Jahn-Teller (JT) active. It induces a structural phase transition from the room-temperature cubic structure into an orthorhombic and orbitally ordered phase ($Imm2$) at $T_{JT} \approx 30$ K [12,22,23]. Figure 1 shows the high-temperature phase of GeV$_4$S$_8$ with the V$_4$S$_4$ cubane clusters and GeS$_4$ tetrahedra. The vanadium ions in the V$_4$ molecules of the cubane clusters constitute a unique electron density resulting in an electronic level scheme as shown in Fig. 1(b) [3].

In the orbitally ordered phase, the V$_4$ tetrahedra distort with one short and one long V-V bond on adjacent sites [23] thereby inducing long-range FE order [12,15,24]. GeV$_4$S$_8$ exhibits an antiferromagnetic (AFM) ground state in contrast to the ferromagnetic (FM) arrangement revealed in the majority of the lacunar spinels. The AFM order is established below 13–18 K [15,21] with the space group P_bmn2_1 describing the

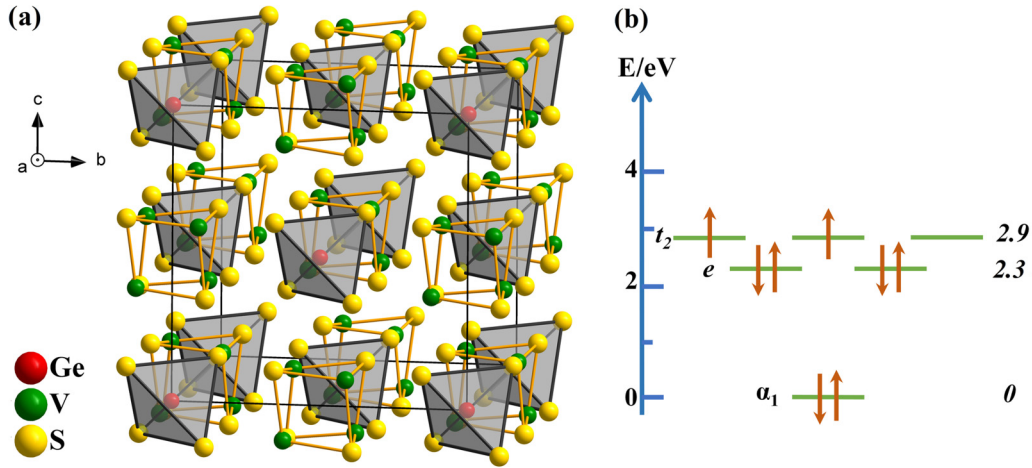*Corresponding author: vladimir.tsurkan@physik.uni-augsburg.de

FIG. 1. (a) Crystallographic structure of the high-temperature phase of the lacunar spinel GeV_4S_8. The constituting ions are colored as indicated in the figure. Yellow bars indicate the V_4S_4 cubane clusters, black bars the GeS_4 tetrahedra, which are light gray colored. The solid black lines, which constitute a cube, indicate the *fcc* high-temperature structure of the lacunar spinels. a, b, and c correspond to the crystallographic axes of the cubic cell. (b) Level scheme of the V_4 clusters with a unique electron and spin density. The figure has been adapted from Ref. [3]. The eight electrons of the vanadium cluster are distributed among the singlet, the doublet, and the triplet, with two electrons in the excited triplet constituting a spin $S = 1$, and hence, these clusters are Jahn-Teller active.

symmetry of the magnetically ordered phase [21]. Later, it was concluded that the AFM order appeared without symmetry changes but only increased the existing distortions [23].

Recent structural, electrical resistivity, magnetization, specific heat, and dielectric studies of GeV_4S_8 provided a detailed characterization of the single crystals also used in the present experiments [15]. In these samples, the onset of AFM order is detected at 14.6 K, while the JT-derived structural phase transition occurs at 30.5 K. The magnetic susceptibility follows a Curie-Weiss (CW) law, with a PM moment of 2.84 μ_B and a CW temperature of -43 K, for data analyzed between 30 and 100 K. The effective moment corresponds to a spin $S = 1$ system, assuming a spin-only g value of 2. It is important to note that the JT transition induces a significant first-order-like jump of the magnetic susceptibility. Below the transition at 30.5 K, the CW temperature changes to -67 K.

These macroscopic measurements were supplemented by THz time-domain spectroscopy revealing a complex behavior of the low-lying phonon excitations, closely linked to the onset of the orbitally driven ferroelectricity [24,25]. Abrupt changes in the dielectric constant show that the onset of orbital order appears via a structural phase transition with strongly first-order character and that AFM order is accompanied by significant structural changes, which are of first-order character too [15]. To provide further insight into the magneto-elastic coupling and the origin of the ferroelectric and antiferromagnetic phase transitions we performed a high-magnetic-field study of single crystalline GeV_4S_8 utilizing ultrasound propagation, magnetization, and dielectric polarization measurements. Studies of the evolution of structural, magnetic, and polar phases as function of temperature and magnetic field are rare and are of fundamental interest in systems with competing orbital, spin, and polar order parameters. In this work, we evidence a complex (H,T) phase diagram and unconventional field-induced transitions with large temperature and field hystereses, which reflect the structural relaxation dynamics in the molecular-cluster units. In addition, it is an

intriguing question if the orbital order in GeV_4S_8 can be suppressed in high magnetic fields. Investigations of magnetic field effects on Jahn-Teller transitions are rare and were performed mainly on $4f$ systems with much lower orbital ordering temperatures. In d derived transition-metal compounds, JT energies usually are much larger than the magnetic energies that can be reached even in magnetic high-field laboratories. In the present experiments, the magnetic-field strength ($\sim$60 T) significantly exceeds the corresponding orbital ordering temperature ($\sim$30 K), and we can expect that the external magnetic field significantly acts on the spin as well as on the orbital degrees of freedom. Furthermore, in GeV_4S_8 orbital order is coupled to the appearance of polar order, which makes this system even more exotic and the (H,T) phase diagram more complex.

II. EXPERIMENTAL DETAILS

Single crystals of GeV_4S_8 were grown from polycrystalline material by chemical transport reactions utilizing iodine as transport agent. A detailed synthesis route as well as a thorough structural, magnetic, thermodynamic, and dielectric characterization is reported in Ref. [15]. High-field experiments were performed at the Dresden High Magnetic Field Laboratory. The pulsed-field ultrasound measurements used magnetic field pulses with a duration of 150 ms and a characteristic rise time of 35 ms. The high-field magnetization was investigated in pulsed magnetic fields up to 60 T with duration of pulses of 25 ms using a compensated pick-up coil system [26]. The temperature and magnetic-field-dependent elastic properties were studied by measurements of the velocity and attenuation of longitudinal and transverse ultrasound waves with the wave vector, **k**, parallel to the ⟨111⟩ axes. Assuming cubic crystal symmetry at all temperatures and fields, the longitudinal mode is related to the elastic constant $c_L = (c_{11} + 2c_{12} + 4c_{44})/3$, while the transverse mode to $c_T = (c_{11} - c_{12} + c_{44})/3$. The measurements were performed

in static magnetic fields up to 15 T for temperatures between 1.5 and 300 K, and in pulsed magnetic fields up to 62 T from 1.3 to 40 K. In the ultrasound experiments the external magnetic field was parallel to the crystallographic $\langle 111 \rangle$ direction. These systematic high-field experiments were supplemented by some measurements of the longitudinal and transverse sound velocities for the ultrasound propagation along the $\langle 100 \rangle$ direction. A standard pulse-echo method [27] with phase-sensitive detection technique was used in all reported ultrasound measurements. The FE polarization was measured via a pyroelectric technique [28] with silver-paste electrodes on both sides of the sample. In these experiments, the polarization or depolarization current is detected that corresponds to the time derivative of the polarization. This method is perfectly compatible with measurements in pulsed fields yielding strongly enhanced time derivatives [29]. The pyrocurrent was mainly measured along the $\langle 111 \rangle$ direction, parallel to the external magnetic field using a digital oscilloscope with high sampling rate. The sample was a platelet with plane-parallel surfaces of $1.8\,\text{mm}^2$ and a thickness of 0.39 mm. After each pyrocurrent measurement, the sample was heated up to 50 K and then cooled down applying a voltage of 39 V. During the pulsed-field experiments, the voltage was switched off. The resulting FE polarization was calculated numerically by integrating the pyrocurrent. Magnetization studies in megagauss fields were performed at the National Laboratory for High Magnetic Fields, Toulouse. In these experiments, the duration of the field pulses was 2 μs.

III. EXPERIMENTAL RESULTS AND DISCUSSION

A. Ultrasound experiments

Ultrasound experiments are ideally suited to detect structural and magnetic phase transitions as function of temperature and external magnetic field and are a perfect tool to determine (H,T) phase diagrams [30]. Due to lattice distortions at cooperative JT transitions, temperature and field-dependent ultrasound measurements provide detailed insights into the leading microscopic mechanisms at these transitions.

1. Ultrasound experiments in static magnetic fields

In a first step, we performed experiments to determine the temperature and field dependence of the longitudinal and transverse sound velocities in moderate static magnetic fields. Figure 2 shows the temperature dependence of the transverse sound velocity in GeV_4S_8 for the sound wave propagating along the crystallographic $\langle 111 \rangle$ direction in zero external magnetic field. Below room temperature and on decreasing temperatures, the sound-velocity $\Delta v/v$ exhibits a large and continuous softening of ~12%. At the structural orbital-order driven phase transition at $T_s \approx 30$ K, $\Delta v/v$ shows a sharp and deep minimum, followed by a significant increase on further decreasing temperatures in the orbitally ordered phase. At the AFM transition at $T_N \approx 15$ K, the sound velocity reveals a small steplike increase and tails off towards lowest temperatures. The anomalous features revealed in the sound velocity at T_N and T_s are accompanied by significant anomalies in the temperature dependence of the sound attenuation $\Delta\alpha$. A substantial thermal hysteresis on heating and cooling was
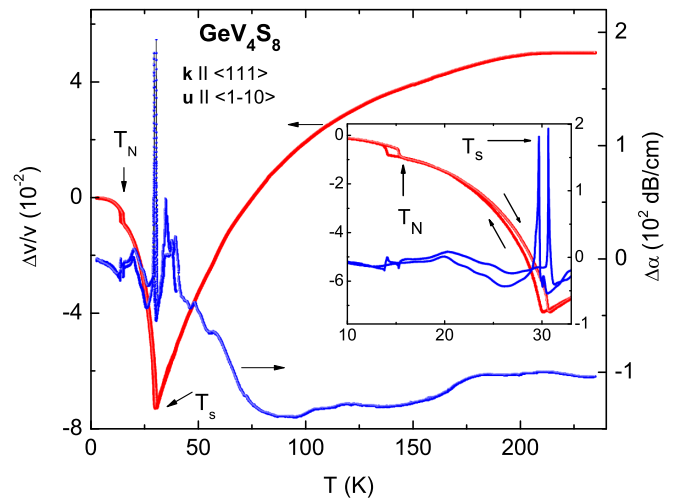

FIG. 2. Relative change of the temperature-dependent sound velocity $\Delta v/v$ (left scale) and of the sound attenuation $\Delta\alpha$ (right scale) of the transverse acoustic mode propagating along the $\langle 111 \rangle$ direction in zero magnetic field in single-crystalline GeV_4S_8. Sound velocity and damping were normalized at the lowest temperatures. The structural T_s and magnetic T_N phase-transition temperatures are indicated. The inset shows the anomalous damping at the phase transitions with hysteretic behavior on an enlarged scale. Here the arrows indicate ordering temperatures as well as heating and cooling directions.

observed for both phase transitions in $\Delta v/v$, as well as in $\Delta\alpha$. These hysteresis effects at the structural and magnetic phase transitions evidence a strong first-order character of both transitions, which is in agreement with results of specific-heat studies [15].

We would like to recall that the overall temperature dependence of the transverse sound velocity in GeV_4S_8—as presented in Fig. 2—resembles prototypical features of JT phase transitions, as found for instance, in a variety of rare-earth vanadates [30]: a continuous softening of the acoustic mode when approaching the phase transition from above, and a steep increase below the transition to the orbitally ordered phase. Please note that in $4f$ systems JT transitions sometimes are named quadrupolar phase transitions, while in $3d$ they usually are termed orbital-order transitions. In the further course of this work including the magnetic field-dependent measurements, this characteristic softening of the appropriate sound velocities will serve as an indication for orbital ordering at the JT transition.

Figure 3 shows the temperature dependence of the velocity of the longitudinal acoustic mode propagating along the $\langle 111 \rangle$ direction for magnetic fields of 0, 5, and 10 T applied as well parallel to $\langle 111 \rangle$. In these experiments, the JT transition appears close to 31 K and AFM order is established at 15 K, with both transition temperatures roughly independent on the magnetic field. In distinction to the behavior found for transverse sound waves, $\Delta v/v$ for the longitudinal waves reveals a steplike increase at the structural phase transition, followed by a smaller increase at the onset of AFM order. Again, both transitions are slightly hysteretic, with hysteresis loops of 2 K width. The sound velocity along
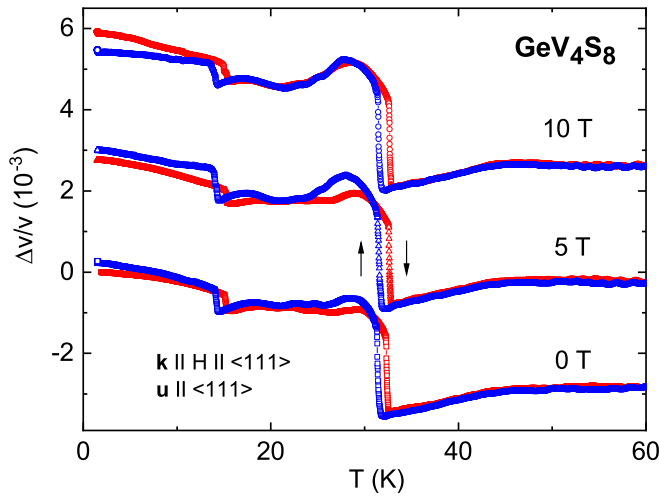
FIG. 3. Relative change of the sound velocity $\Delta v/v$ of the longitudinal acoustic mode propagating along the $\langle 111 \rangle$ direction vs temperature in external magnetic fields of 0, 5, and 10 T, in single crystalline GeV_4S_8. The arrows indicate heating and cooling direction. All data were normalized to zero relative change for the measurements on heating in zero external magnetic fields. For clarity, the curves at 5 and 10 T are shifted with respect to the vertical axis.

$\langle 111 \rangle$ increases by approximately 0.3% just at the orbital ordering transition and reaches higher values in the orbitally ordered state.

In all further analysis, it is important to take this significant difference in the behavior of longitudinal and transverse sound waves at the JT phase transition into account: Obviously, the transverse sound mode reveals a clear softening when approaching the structural phase transition from above and below. Longitudinal sound waves along $\langle 111 \rangle$ exhibit a steplike change of the velocity only, with a slightly enhanced sound velocity in the orbitally ordered phase. The relative velocity changes of the latter are roughly by a factor of 10 smaller than the overall softening of the transverse sound mode.

2. Ultrasound experiments in pulsed magnetic fields

Figure 4 presents the field dependence of the sound velocity of the transverse acoustic mode propagating along the $\langle 111 \rangle$ direction at several temperatures in the magnetically and orbitally ordered phase in pulsed magnetic fields up to 62 T. Figure 4(a) shows the relative change of the velocity of the transverse sound below and around the onset of AFM order. On increasing fields, the transverse sound velocity reveals a slight increase (1.4 K) or remains almost temperature independent (11 and 15.2 K) before significant softening appears for further close to 46 T and increases again for further increasing fields. This minimum becomes broadened, shifts to lower fields on increasing temperatures, and is located at 33 T at 15.2 K. On decreasing fields, extreme hysteresis effects appear and the sound velocity passes through broad minima, significantly shifted to lower fields, compared to the up-sweep data. In detail, the minimum shifts from 46 T for fields sweep up to 32 T for field sweep down. Specifically, the sound velocity does not reach values identical or even close to the starting point of the experiment. This fact indicates that
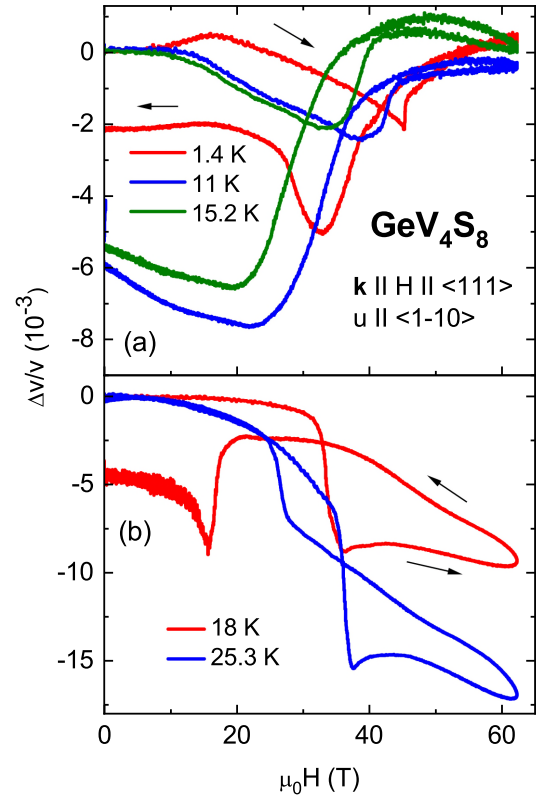

FIG. 4. Relative change of the sound velocity $\Delta v/v$ of the transverse acoustic mode along $\langle 111 \rangle$ vs magnetic field for GeV_4S_8 at a series of temperatures crossing the structural and magnetic phase transitions: (a) below and close to the zero-field AFM phase transition at T_N and (b) in the zero-field paramagnetic, but still orbitally ordered phase. Arrows indicate measurements for up and down-field sweeps. In all experiments, at the structural phase transitions, extreme hysteretic behavior occurs, indicating that the experiments may not always have been conducted in thermal equilibrium (see text).

on the timescale of the experiment, i.e., on the few hundred millisecond timescale, metastability is found and the material does not reach thermodynamic equilibrium during the pulsed field scans. These features indicate dynamic processes, which will show up in all further experiments of this work. This extreme hysteretic behavior with indications that thermal equilibrium is not always reached, results from a combination of first-order effects at the structural phase transitions, with structural relaxation processes, which obviously are slower than the pulse duration. In the Appendix it is documented that for magnetic-field cycles not crossing structural phase transitions, the experiments are always close to thermal equilibrium and up and down sweeps are rather reproducible. This is also the reason why we decided to construct the phase diagram from critical temperatures determined in the field-up cycles, which seems to be least affected by these effects.

Compared to the field sweeps in the AFM phase, even more dramatic changes in the field dependence of the transverse sound velocities show up in the orbitally ordered but paramagnetic (PM) phase, implying that the structure or at least the spin-lattice coupling in the PM and AFM phases has changed considerably. In the PM regime, the
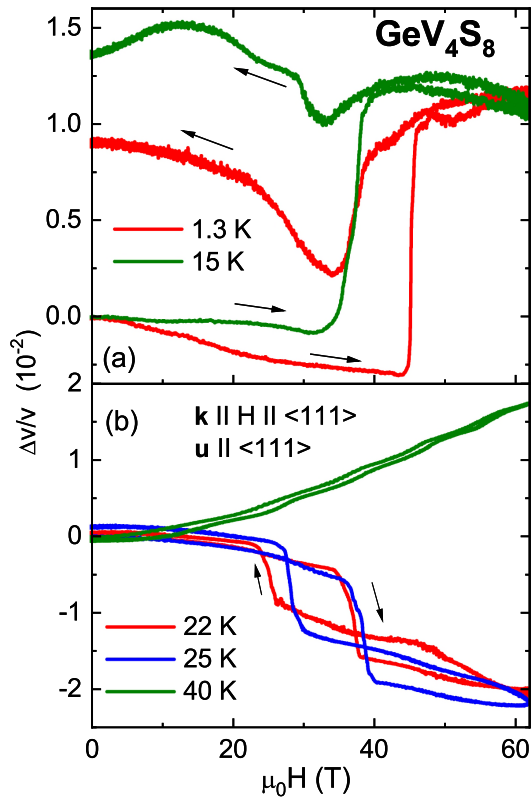
FIG. 5. Relative change of the sound velocity $\Delta v/v$ of the longitudinal acoustic mode along $\langle 111 \rangle$ vs magnetic field for GeV_4S_8 at a series of temperatures crossing the structural and magnetic phase transitions: (a) below and close to the zero-field antiferromagnetic (AFM) transition at T_N and (b) in the zero-field paramagnetic (PM) phase.

relative changes of the sound velocities as measured at 18 and 25.3 K are plotted in Fig. 4(b). At 18 K and on increasing fields, the sound velocity remains almost constant, exhibits a steplike decrease of approximately 1% close to 35 T and then remains constant for further increasing fields up to 60 T. A similar behavior is found for the field dependence at 25.3 K. The acoustic mode starts to soften already at lower fields, shows a steplike decrease at slightly higher fields and remains rather constant for further increasing fields. Again, enormous hysteresis effects appear on decreasing fields, connected with the first-order structural phase transition, indicating that the system has fallen out of thermodynamic equilibrium, which cannot be reached on the timescale of the experiment, which is set by the pulse length of the magnetic field pulses. On decreasing fields, we find a continuous increase of the relative sound velocity, a sharp diplike minimum close to 15 T at 18 K, and a steplike increase for the transverse sound velocities measured at 25.3 K. Compared to the steplike decrease in the up sweeps, the steplike increase in the down sweeps is shifted to significantly lower fields. It is remarkably that at 25.3 K thermal equilibrium can be reached at low fields with very similar behavior of the sound velocity for up and down sweeps.

Figure 5 shows the field dependence of the sound velocity of the longitudinal acoustic mode propagating along the $\langle 111 \rangle$ direction at several temperatures in pulsed magnetic fields up

to 62 T. Figure 5(a) shows the field-induced sound-velocity changes in the magnetically ordered phase. At the lowest measured temperature of 1.3 K, for increasing field, the sound velocity manifests a sharp jumplike increase of more than 1% at 46 T. At 15 K, this anomaly is shifted to significantly lower fields. Again, for down-sweep cycles strong hysteresis effects are observed, evidencing first-order effects with the observation that thermal equilibrium cannot be reached on the timescale of the experiment. In Fig. 5(b) the relative changes of the longitudinal sound velocities in the paramagnetic phase are shown. On increasing fields, now the changes of the sound velocity are opposite compared to the effects in the AFM phase: For up sweeps, $\Delta v/v$ shows a strong softening close to 38 T and a continuous decrease for further increasing fields. A canonical hysteretic behavior appears for down sweeps. It seems that in these experiments on the timescale of the field changes, the sample comes close to thermodynamic equilibrium. At 40 K, the sound velocity shows a continuous and moderate increase with increasing fields. Up- and down-sweep cycles reveal very similar results evidencing that above the structural phase transition the samples are in thermodynamic equilibrium and behave like regular solids far from any structural anomaly.

Comparing these magnetic field-dependent ultrasound experiments, we have to admit that it seems rather impossible to arrive at definite and final conclusions concerning the nature of some of these JT derived phase transitions. First, from the very different field dependencies of the sound velocities in the PM ($15 < T < 30$ K) as well as in the AFM phase ($T < 15$ K) we assume two different orbitally ordered states in these temperature regimes and at low fields. These phases with different orbital orders (OO) will be indexed as OO1 ($15 < T < 30$ K) and OO2 ($T < 15$ K) in the phase diagram. Furthermore, experiments beyond 15 K, in the paramagnetic and orbitally ordered low-field phase OO1, transverse [Fig. 3(b)] and longitudinal [Fig. 4(b)] sound experiments reveal a jumplike decrease of velocities when passing into the orbitally disordered phases on increasing fields. This behavior reconciles the effects documented the temperature-dependent measurements of the longitudinal sound, revealing a stiffer lattice in the OO1 phase (Fig. 3). In the low-temperature experiments, starting in the orbitally ordered and AFM phase OO2, the transverse velocities reveal rather a softening effect [Fig. 3(a)] in accordance with the temperature-dependent measurements (Fig. 2); however, the longitudinal sound increases when passing the phase boundary from orbital order to orbital disorder. This behavior remains unexplained. One could speculate that below 15 K a second orbitally ordered phase, with different orbital order, follows the low-field OO2 phase. However, this possibility seems unlikely in the light of magnetization and pyrocurrent measurements. This high-field phase is nonpolar, and it seems that in lacunar spinels all orbitally ordered phase are ferroelectric.

B. High-field magnetization

As outlined above, Widmann et al. [15] reported detailed measurements of the temperature dependence of the magnetic susceptibility crossing the structural and magnetic phase transition of GeV_4S_8. Figure 6 shows the
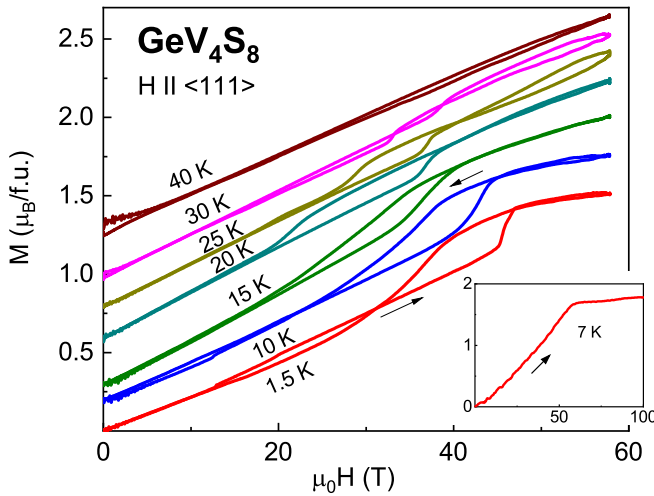
FIG. 6. Magnetization M vs magnetic field H for single crystalline GeV_4S_8 measured along the $\langle 111 \rangle$ direction at a series of temperature between 1.5 and 40 K. For clarity, the curves are shifted by approximately by $0.2\,\mu_B$ along the vertical axis. Arrows indicate the field-sweep directions. The inset shows a magnetization measurement up to 100 T at 7 K to document the transition into the polarized ferromagnetic phase just above 60 T.

magnetic-field dependence of the magnetization M, measured in pulsed magnetic fields applied along the $\langle 111 \rangle$ direction at various temperatures between 1.5 and 40 K, covering the magnetically as well as the orbitally ordered phases. At 1.5 K and in the up-sweep cycle, a linear increase of magnetization up to $\sim$13 T is followed by a slightly increasing slope, indicating an incipient metamagnetic transition. A pronounced jump at 46 T interrupts the subsequent linear increase of the magnetization. After this metamagnetic transition, the magnetization levels off approaching a value close to $1.5\,\mu_B$. It is important to note that the saturated magnetization is well below the fully field-polarized ferromagnetic moment, which is expected to be close to $2\,\mu_B$ for a $S = 1$ magnet. On decreasing field, a prominent hysteresis evolves extending down to 31 T, followed by a smaller hysteresis, which closes at 13 T. This small hysteresis is outside experimental uncertainties. In the course of this work, we also identified small anomalies at similar temperatures in the polarization experiments (see below). Finally, the magnetization recovers the linear dependence characteristic for the AFM ground state. Already at this point we would like to state that the characteristic hysteresis, which evolves in these high-field magnetization experiments between 20 and 40 T signals magnetization changes due to suppression and recovery of orbital ordering (OO) rather than an AFM hysteresis loop. This we will detail in the following.

To check whether the saturation magnetization at high fields corresponds to the fully ordered spin moment of the molecular V_4 cluster, we performed pulsed-field experiments up to 100 T. Data at 7 K are shown in the inset of Fig. 6. Indeed, a saturation of the magnetization is observed close to 60 T, indicating a fully field-polarized ferromagnetic state. It is unclear, why the saturated moment is well below the $S = 1$ value, which was identified in the high-temperature CW behavior [15]. It may be that the molecular vanadium clusters,

with a common electron density constituting a molecular $S = 1$, are no more stable at these high magnetic fields. We also have to admit that there is no perfect agreement between the 60 and 100 T experiments. The transitions in the latter experiment are much more broadened and there is no steplike increase of the magnetization close to 46 T as documented in the main frame of Fig. 5. This behavior may result from the different timescales of the field pulses in these two types of experiments.

With increasing temperatures up to 15 K, the dominating high-field hysteresis extends over a larger field range and then becomes narrower again. Above 30 K, the magnetization is close to linear in the complete field range measured, with no indication of saturation. It is also evident that the incipient metamagnetic transition, at 13 T ($T = 1.5$ K), becomes suppressed at higher temperatures and cannot be identified at 15 K anymore. As a working hypothesis, we conclude that the significant high-field hysteresis marks the JT-derived structural phase transition: On increasing fields, OO seems to become destroyed at high magnetic fields beyond 45 T. On decreasing fields, OO is reestablished at significantly lower fields. As reported in Ref. [15], AFM order only exists below 15 K and remains almost unchanged in external magnetic fields up to 9 T. This is in accordance with the experimental observations in the sound velocity experiments (Fig. 3).

C. Ferroelectric polarization as function of temperature and magnetic field

Figure 7 shows the magnetic-field dependence of the ferroelectric polarization in GeV_4S_8 measured in pulsed fields up to 60 T for a series of temperatures between 1.4 and 30 K. As outlined above, the FE polarization was determined by integrating the magneto-current for up- and down-field sweeps. In all field-dependent experiments, it was assumed that a paraelectric (PE) phase with zero polarization is reached above 60 T. Representative results are shown separately for temperatures below the magnetic ordering temperature T_N [Fig. 7(a)] and below 30 K, in the orbitally ordered but PM phase [Fig. 7(b)].

Three striking phenomena have to be mentioned:

(i) Strong field-dependent hystereses appear at all temperatures. For all temperatures shown, the polarization at the end of the field-sweep cycle is not completely recovered documenting that thermal equilibrium is not reached on the timescale of these pulsed experiments. This behavior follows from the fact that ferroelectricity is induced via a first-order structural phase transition establishing OO as well. Obviously, compared to the timescale of the magnetic pulses, the structural relaxation times are too long to establish thermal equilibration in these field cycles. It is important to note that the measurements of the magnetocaloric effect performed on these GeV_4S_8 crystals (see the Appendix) allow to conclude that the hysteresis observed in all pulsed-field experiments (ultrasound, magnetization, and polarization) is related to dynamical effects due to the first-order phase transition, which hinder thermal equilibration on short timescales. As documented in Fig. 9(a) below, when no structural relaxation is crossed in a field cycle, the temperature remains close
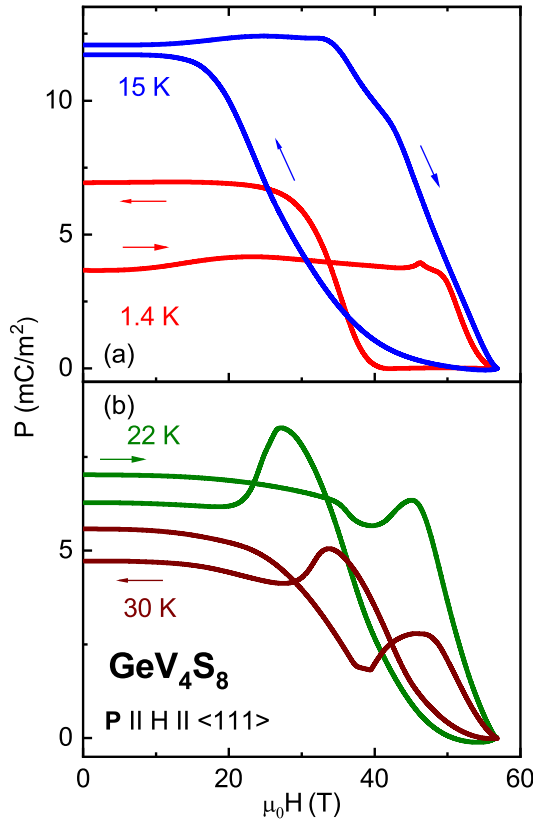
FIG. 7. Ferroelectric polarization P vs magnetic field H measured along $\langle 111 \rangle$ for different temperatures for GeV_4S_8. In all experiments shown, the external field was applied parallel to the electric field direction. (a) Polarization experiments below 15 K in the magnetically ordered phase. (b) FE polarization in the PM phase. In all panels, the arrows indicate the field sweep directions. In all field-dependent measurements, it was assumed that a paraelectric (PE) phase with zero polarization is reached above 60 T.

FIG. 8. (H,T) phase diagram of single crystalline GeV_4S_8 with the external magnetic field applied along the $\langle 111 \rangle$ direction. The anomalies detected during up sweeps are used to construct the phase diagram. The anomalies as determined in static (s) and pulsed (Us) ultrasound experiments utilizing longitudinal (L) and transverse (T) sound waves are indicated together with anomalies from magnetization (M) and pyrocurrent (P) experiments. Anomalies from heat-capacity experiments (C_p) by Widmann *et al.* [15] are indicated as well. Magnetic phases: antiferromagnetic (AFM), paramagnetic (PM), and field-induced ferromagnetic (FM) phases were determined. In addition, a zoo of polar phases, paraelectric (PE), ferroelectric (FE1–FE3), as well as orbitally disordered (OD), and orbitally ordered (OO1–OO2) phases, were identified. Solid lines serve as guides to the eye. As documented in the field-dependent experimental results, the measurements were not always performed in thermal equilibrium. For this reason, only critical temperatures in up-field cycles are shown in this phase diagram.

to isothermal and up- as well as down-sweeps are almost identical.

(ii) There is a significant difference for the field sweeps performed in the magnetically ordered [Fig. 7(a)] and in the PM phase [Fig. 7(b)]. The polarization experiments below 15 K show one dominating hysteresis and minor anomalies close to 20 T. In the orbitally ordered but PM phase, a well-developed second FE phase appears beyond 40 T. For low increasing fields, the polarization in the orbitally ordered phase continuously decreases, but then is followed by a second FE phase.

(iii) When comparing results from the pyroelectric measurements at 22 K with those of the sound-velocity experiments [Fig. 5(b)] at the same temperature, it seems that the dominating structural phase transition corresponds to the first polarization anomaly, while a second FE phase extends up to much higher fields. At present, this behavior is not fully understood: It is unclear if this high-field FE phase is accompanied by a different orbital-order pattern. The strong irreversibilities detected in the ultrasound experiments at high fields [Figs. 4(b) and 5(b)] are in favor for this interpretation. Alternatively, one could assume that this high-field FE polarization exits in an orbitally disordered phase and is
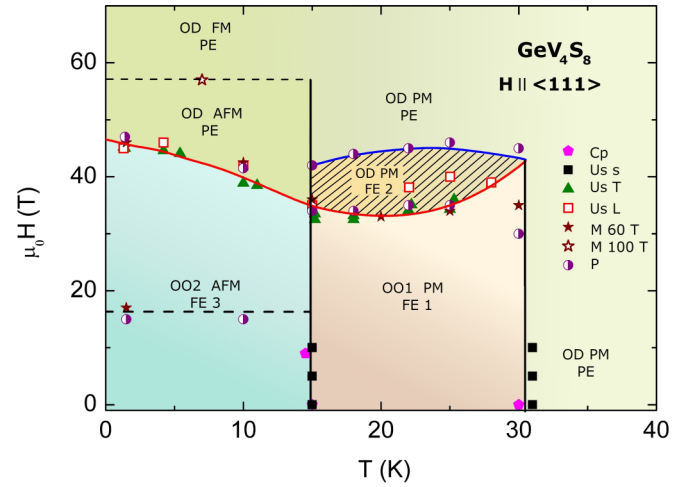
induced, e.g., by spin degrees of freedom. Additional high-field experiments and theoretical support is needed to clarify this point.

D. (H, T) phase diagram of GeV_4S_8

Figure 8 summarizes the results of the present high-field studies showing the (H,T) phase diagram obtained for GeV_4S_8 and field applied along the $\langle 111 \rangle$ direction. To exclude complications due to strong hysteresis and nonequilibrium effects, we used the data only for field-sweep up cycles. At low fields and above ~ 30 K a PE, PM, and orbitally disordered (OD) phase as the stable state is well established. Indeed, in all field sweeps above 30 K, we observed a continuous evolution of sound velocity, magnetization and polarization with no apparent anomalies. At ~ 30 K a first-order JT transition induces OO and a FE polarization. In the phase diagram, this phase is characterized by OO1 and FE1. This orbitally ordered phase is stable up to 46 T, a critical field where sound-velocity and magnetization experiments indicate the suppression of the OO. Astonishingly, a second FE phase, FE2, exists even at higher fields and is stable up to 50 T. We however cannot exclude that the region between OO1-PM-FE 1 phase and OD-PM-PE phase can define a metastable phase due to first-order origin of the transition between these phases. This question needs further study.

The phase diagram changes significantly with the onset of AFM order at 15 K. The OO changes, a fact, which most drastically is indicated by the field-dependent sound propagation of longitudinal sound waves (Fig. 5). In the PM phase, the sound velocity exhibits a jumplike decrease at the onset of OO, while in the AFM phase the sound velocity increases at this phase boundary. In the phase diagram, this phase is indicated as OO2. In addition, also the polarization reveals a different field-dependent characteristic, providing a fingerprint for a FE phase FE3. This polar phase seems to undergo slight changes just below 20 T and is followed by an OD and PE phase above ∼40 T. From high-field experiments of the magnetization up to 100 T we identify the phase boundary to the field-induced FM and PE phase close to 60 T.

IV. CONCLUDING REMARKS

In the course of this work, we performed a comprehensive high-field study of the lacunar spinel GeV_4S_8. Lacunar spinels are a highly interesting class of materials with molecular units as structural building blocks. Specifically, vanadium V_4 clusters are characterized by a unique electron distribution establishing a spin $S = 1$ per molecule. Most of the lacunar spinels are JT active with orbital-order transitions of the order of 30 K. Interestingly, the JT transition in this class of compounds induces ferroelectricity via specific distortions of the vanadium tetrahedra. As function of temperature and magnetic field, the present work revealed a complex phase diagram including magnetic, ferroelectric, multiferroic and orbitally ordered phases. The complexity of the (H,T) phase diagrams in spinel compounds has recently been documented by the observation of multiferroic spin-superfluid and spin-supersolid phases in $MnCr_2S_4$ [31,32].

The high-field studies of this work were motivated by the relatively low orbital ordering temperatures of the lacunar spinels and by the fact that nowadays magnetic field energies, which can be reached in high-field laboratories, significantly can overcome the JT energies. In addition, in the title compound the JT phases are ferroelectric and the orbitally ordered phases can be identified utilizing sound-wave experiments as well as pyrocurrent measurements. Reviews on the physics of the Jahn-Teller effect were published by Gehring and Gehring [33], by Kugel and Khomskii [34] as well as by Goodenough [35]. The theoretical concept has been outlined by Pytte [36] and later was extended to include external magnetic fields [37]. References [34] and [37] document the complexity of an adequate modeling of these systems with two coexisting order parameters: the orbital structure and the spin order depend on each other in magnetic materials, which contain ions having an orbitally degenerate ground state and this interrelation leads to nontrivial and exotic orbital and magnetic structures. In GeV_4S_8 this complexity is even enhanced by the fact that the orbitally ordered phases are polar and that the electronic level scheme, as documented in Fig. 1(b) corresponds to a unique electron distribution of a complex vanadium molecule constituting spin $S = 1/2$. Schematic (H,T) phase diagrams of JT systems, which are documented in [34] and [37], depend on the crystal symmetry, on the field direction and on the specific level splitting of the JT active ion in the crystal electric field of the host, in most cases are heavily oversimplified.

So far, experimental work on JT systems in magnetic fields mainly was restricted to $4f$ compounds with much lower orbital ordering temperatures. Indeed, in TmV_2O_4 with a JT transition of 6 K, it has been shown that orbital order can be suppressed in critical magnetic fields of approximately 2 T [38]. So far, similar experiments are missing in in transition-metal oxides with $3d$ ions and first attempts are documented in this manuscript. Any theoretical interpretation of the complex observed effects is certainly far outside the scope of this work.

We performed detailed ultrasound experiments, following the field evolution of longitudinal and transverse sound waves up to 60 T. In addition, we investigated the magnetization and FE polarization in external fields up to 60 T. These studies were complemented by ultrasound experiments in static magnetic fields up to 15 T. The experiments in static and pulsed magnetic fields allowed the construction of a $(H\text{-}T)$ phase diagram documenting a sequence of magnetic, polar, and orbitally ordered phases. Specifically, we revealed the appearance of two orbitally ordered phases OO1 and OO2, in addition to the orbitally disordered (OD) phases at high fields (>50 T) and high temperatures (>30 K). We evidenced a zoo of ferroelectric phases, FE1, FE2, and FE3, in addition to the PE phase at high fields (>50 T) and high temperatures (>15 K). Finally, the polarized FM phase for fields above 60 T is identified in addition to the AFM phase and the PM phase for temperatures for temperatures higher than 15 K. At low temperatures and for fields below 40 T, AFM order coexists with the polar phase FE3, hence constituting a multiferroic phase. Many of the high-field phases reveal significant hysteresis with metastable phase regimes where thermodynamic equilibrium cannot be reached on the timescale of the pulse-field cycles. It is worthwhile to compare the present results with a similar high-field study in the multiferroic normal spinel $CoCr_2O_4$ [39], where ferromagnetic spin order is followed by a conical spiral with FE polarization [40]. Similar to observations in the title compound, also in this normal spinel an extreme metastable high-field phase was identified which was completely frozen in after applying large field pulses.

APPENDIX: MAGNETOCALORIC EFFECT IN PULSED MAGNETIC FIELDS

Adiabatic temperature changes observed in pulsed magnetic fields [magnetocaloric effect (MCE)] in GeV_4S_8 were measured for both magnetic field configurations, $\mathbf{H} \parallel \langle 111 \rangle$ and $\mathbf{H} \parallel \langle 100 \rangle$, respectively. These measurements of the

MCE were performed to document that the significant hysteresis effects observed in various pulsed magnetic-field experiments (ultrasound, magnetization, and polarization) stem from dynamical effects related to first-order phase transition. When passing these critical temperatures the coupled spin-lattice system falls out of thermal equilibrium, and in specific cases, equilibration cannot be reached at the timescale of the pulsed experiments.

MCEs were measured by using a RuO_2 thermometer (900 ohm at 4 K, $0.6 \times 0.3 \times 0.1 \, mm^3$; for details see Refs. [41,42]). To achieve adiabatic conditions, the sample was placed in a vacuum environment. The thermometer was glued on the polished surface of the single crystal. The resistance of the thermometer was measured with a standard *ac* four-probe method using a numerical lock-in technique at the frequency of 50 kHz. The results were obtained at temperatures only below 15 K, which is the sensitivity limit of the RuO_2 thermometer used in these experiments.

Figures 9(a) and 9(b) show the results for magnetic field directions **H** ∥ ⟨111⟩ and **H** ∥ ⟨100⟩, respectively. The critical fields at the phase transitions are very close for both geometries. The low-temperature results for $T < 5$ K show clear anomalies, which are related to the phase transition from the OO and FE to the OD and PE phase (see main text). In the field-down sweeps, the temperature shows completely different magnetic-field dependence with significant hysteresis. For both geometries the sample remains at a much higher temperature. This out-of-equilibrium behavior is observed in the other pulsed field measurements, like ultrasound or polarization, as well. The temperature difference between the up and the subsequent down cycle is of order 5 K at the lowest temperature
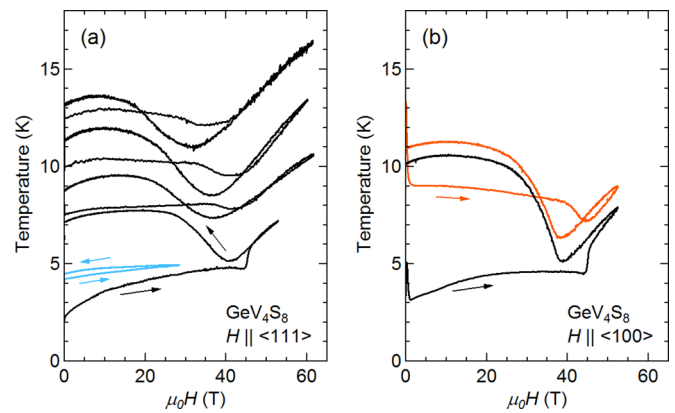

FIG. 9. Adiabatic temperature changes of GeV_4S_8 measured in pulsed magnetic fields for (a) **H**∥ < 111 > and (b) **H**∥ < 100 >. The results for the selected initial temperatures are shown. The arrows show the field-sweep directions.

and becomes smaller at higher temperatures. These heating effects cannot be explained in terms of canonical hysteresis effects at first-order phase transitions, but signal that the sample falls out of thermal equilibrium and that equilibration cannot be achieved at the timescale of the pulsed experiment. In other words, the system does not have enough time to relax to the ground state and the phase transition occurs in a metastable manner. Note that these dynamical effects are only observed when passing critical fields characteristic for phase transitions. When in field-cycling experiments the maximum field is small [see cyan curve in Fig. 9(a)], within experimental uncertainties the field cycling results are reversible.

[1] H. Barz, Mat. Res. Bull. **8**, 983 (1973).

[2] J. M. Vandenberg and D. Brasen, J. Solid State Chem. **14**, 203 (1975).

[3] D. Johrendt, Z. Anorg. Allg. Chem. **624**, 952 (1998).

[4] S. Harris, Polyhedron **8**, 2843 (1989).

[5] M. M. Abd-Elmeguid, B. Ni, D. I. Khomskii, R. Pocha, D. Johrendt, X. Wang, and K. Syassen, Phys. Rev. Lett. **93**, 126403 (2004).

[6] V. Ta Phuoc, C. Vaju, B. Corraze, R. Sopracase, A. Perucchi, C. Marini, P. Postorino, M. Chligui, S. Lupi, E. Janod, and L. Cario, Phys. Rev. Lett. **110**, 037401 (2013).

[7] A. Camjayi, C. Acha, R. Weht, M. G. Rodríguez, B. Corraze, E. Janod, L. Cario, and M. J. Rozenberg, Phys. Rev. Lett. **113**, 086404 (2014).

[8] E. Dorolti, L. Cario, B. Corraze, E. Janod, C. Vaju, H.-J. Koo, E. Kan, and M.-H. Whangbo, J. Am. Chem. Soc. **132**, 5704 (2010).

[9] V. Dubost, T. Cren, C. Vaju, L. Cario, B. Corraze, E. Janod, F. Debontridder, and D. Roditchev, Nano Lett. **13**, 3648 (2013).

[10] P. Stoliar, L. Cario, E. Janod, B. Corraze, C. Guillot-Deudon, S. Salmon-Bourmand, V. Guiot, J. Tranchant, and M. Rozenberg, Adv. Mater. **25**, 3222 (2013).

[11] V. Guiot, L. Cario, E. Janod, B. Corraze, V. Ta Phuoc, M. Rozenberg, P. Stoliar, T. Cren, and D. Roditchev, Nat. Commun. **4**, 1722 (2013).

[12] K. Singh, C. Simon, E. Cannuccia, M.-B. Lepetit, B. Corraze, E. Janod, and L. Cario, Phys. Rev. Lett. **113**, 137602 (2014).

[13] E. Ruff, S. Widmann, P. Lunkenheimer, V. Tsurkan, S. Bordács, I. Kézsmárki, and A. Loidl, Sci. Adv. **1**, e1500916 (2015).

[14] Z. Wang, E. Ruff, M. Schmidt, V. Tsurkan, I. Kézsmárki, P. Lunkenheimer, and A. Loidl, Phys. Rev. Lett. **115**, 207601 (2015).

[15] S. Widmann, A. Günther, E. Ruff, V. Tsurkan, H.-A. Krug von Nidda, P. Lunkenheimer, and A. Loidl, Phys. Rev. B **94**, 214421 (2016).

[16] S. Widmann, E. Ruff, A. Günther, H.-A. Krug von Nidda, P. Lunkenheimer, V. Tsurkan, S. Bordács, I. Kézsmárki, and A. Loidl, Phil. Mag. **97**, 3428 (2017).

[17] E. Ruff, A. Butykai, K. Geirhos, S. Widmann, V. Tsurkan, E. Stefanet, I. Kézsmárki, A. Loidl, and P. Lunkenheimer, Phys. Rev. B **96**, 165119 (2017).

[18] K. Geirhos, S. Krohns, H. Nakamura, T. Waki, Y. Tabata, I. Kézsmárki, and P. Lunkenheimer, Phys. Rev. B **98**, 224306 (2018).

[19] I. Kézsmárki, S. Bordács, P. Milde, E. Neuber, L. M. Eng, J. S. White, H. M. Rønnow, C. D. Dewhurst, M. Mochizuki, K. Yanai, H. Nakamura, D. Ehlers, V. Tsurkan, and A. Loidl, Nat. Mater. **14**, 1116 (2015).

[20] S. Bordács, A. Butykai, B. G. Szigeti, J. S. White, R. Cubitt, A. O. Leonov, S. Widmann, D. Ehlers, H.-A. Krug von Nidda, V. Tsurkan, A. Loidl, and I. Kézsmárki, Sci. Rep. **7**, 7584 (2017).

[21] H. Müller, W. Kockelmann, and D. Johrendt, Chem. Mater. **18**, 2174 (2006).

[22] H. Chudo, C. Michioka, H. Nakamura, and K. Yoshimura, Physica B **378**, 1150 (2006).

[23] D. Bichler, V. Zinth, D. Johrendt, O. Heyer, M. K. Forthaus, T. Lorenz, and M. M. Abd-Elmeguid, Phys. Rev. B **77**, 212102 (2008).

[24] S. Reschke, Z. Wang, F. Mayr, E. Ruff, P. Lunkenheimer, V. Tsurkan, and A. Loidl, Phys. Rev. B **96**, 144418 (2017).

[25] M. T. Warren, G. Pokharel, A. D. Christianson, D. Mandrus, and R. Valdés Aguilar, Phys. Rev. B **96**, 054432 (2017).

[26] Y. Skourski, M. D. Kuz'min, K. P. Skokov, A. V. Andreev, and J. Wosnitza, Phys. Rev. B **83**, 214420 (2011).

[27] S. Zherlitsyn, S. Yasin and J. Wosnitza, Low Temp. Phys. **40**, 123 (2014).

[28] Z. Wang, N. Qureshi, S. Yasin, A. Mukhin, E. Ressouche, S. Zherlitsyn, Y. Skourski, J. Geshev, V. Ivanov, M. Gospodinov, and V. Skumryev, Nat. Commun. **7**, 10295 (2016).

[29] M. Tokunaga, Front. Phys. **7**, 386 (2012).

[30] B. Lüthi, *Physical Acoustics in the Solid State*, Springer Series in Solid State Sciences Vol. 148 (Springer Verlag, Berlin, 2005).

[31] V. Tsurkan, S. Zherlitsyn, L. Prodan, V. Felea, P. T. Cong, Y. Skourski, Z. Wang, J. Deisenhofer, H.-A. Krug von Nidda, J. Wosnitza, and A. Loidl, Sci. Adv. **3**, e1601982 (2017).

[32] A. Ruff, Z. Wang, S. Zherlitsyn, J. Wosnitza, S. Krohns, H.-A. Krug von Nidda, P. Lunkenheimer, V. Tsurkan, and A. Loidl, Phys. Rev. B **100**, 014404 (2019).

[33] G. A. Gehring and K. A. Gehring, Rep. Prog. Phys. **38**, 1 (1975).

[34] K. I. Kugel and D. I. Khomskii, Sov. Phys. Usp. **25**, 231 (1982).

[35] J. B. Goodenough, Annu. Rev. Mater. Sci. **28**, 1 (1998).

[36] E. Pytte, Phys. Rev. B **3**, 3503 (1971).

[37] E. Pytte, Phys. Rev. B **9**, 932 (1974).

[38] B. W. Mangum, J. N. Lee, and H. W. Moos, Phys. Rev. Lett. **27**, 1517 (1971).

[39] V. Tsurkan, S. Zherlitsyn, S. Yasin, V. Felea, Y. Skourski, J. Deisenhofer, H.-A. Krug von Nidda, J. Wosnitza, and A. Loidl, Phys. Rev. Lett. **110**, 115502 (2013).

[40] Y. Yamasaki, S. Miyasaka, Y. Kaneko, J.-P. He, T. Arima, and Y. Tokura, Phys. Rev. Lett. **96**, 207204 (2006).

[41] T. Kihara, Y. Kohama, Y. Hashimoto, S. Katsumoto, and M. Tokunaga, Rev. Sci. Instrum. **84**, 074901 (2013).

[42] T. Nomura, Y. Kohama, Y. H. Matsuda, K. Kindo, and T. C. Kobayashi, Phys. Rev. B **95**, 104420 (2017).